ACS APPLIED MATERIALS & INTERFACES

Research Article

www.acsami.org

Investigation of Change in Surface Area and Grain Size of Cadmium Titanate Nanofibers upon Annealing and Their Effect on Oxygen Sensing

Z. Imran, S. S. Batool, M. A. Rafiq,* Kamran Rasool, Mushtaq Ahmad, R. N. Shahid, and M. M. Hasan

Micro and Nano Devices Group, Department of Metallurgy and Materials Engineering, Pakistan Institute of Engineering and Applied Sciences (PIEAS), P.O. Nilore, Islamabad, 45650, Pakistan

Supporting Information

ABSTRACT: We have investigated the phase changes in $CdTiO_3$ nanofibers as the annealing temperature of nanofibers was increased from 600 to 1200 °C. The nanofibers annealed at 600 °C were ilmenite with a very small amount of CdO. Upon annealing at 950 °C, CdO was completely removed. Annealing at 1000 °C yielded pure perovskite nanofibers, and at temperatures above 1100 °C rutile TiO_2 nanofibers were obtained. Brunauer–Emmett–Teller (BET) analysis showed that with increase in annealing temperature the surface area of nanofibers was decreased. The nanofibers annealed at 600 °C have the higher surface area of ~9.41 m^2/g. Then oxygen sensors using $CdTiO_3$ nanofibers annealed at 600 °C (ilmenite) and 1000 °C (perovskite) were fabricated. The sensitivity of the ilmenite nanofibers sensor was 2 times than that of the perovskite nanofibers sensor. The response and recovery times were 120 and 23 s, respectively, for the ilmenite nanofibers sensor, whereas response and recovery times were 156 and 50 s, respectively, for the perovskite nanofibers sensor. Better oxygen characteristics of ilmenite nanofibers are attributed to their large surface area and porosity. Therefore, we believe that ilmenite $CdTiO_3$ nanofibers are potential candidates to develop practical oxygen sensors.

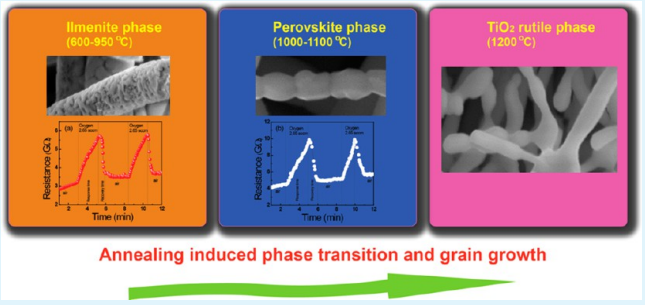

KEYWORDS: *$CdTiO_3$, electrospinning, nanofibers, phase transformation, oxygen sensor*

1. INTRODUCTION

Titanium-based oxides are of great interest due to their diverse applications such as humidity sensors, gas sensors, microelectronic devices, and photocatalytic cells.[1,2] Various synthesis techniques such as hydrothermal crystallization,[3] sol–gel,[4] sputtering,[5] and electrospinning[1,6] have been used to prepare nanostructures of these oxides. Spray pyrolysis has also been used to synthesize TiO_2 thin films and flower-like nanostructures.[7,8] Cadmium titanate ($CdTiO_3$), one of these oxides, has excellent gas sensing, dielectric, and optical properties.[9,10]

Oxygen sensing and leakage from industrial installations is considered a most critical problem to be resolved related to human health, aquatic life, and environmental issues.[6,11] Oxygen leakage may lead to fire and explosion hazards in hyperbaric chambers used in medical treatment, food preservation and packing, steel works, and chemical plants.[12,13] Moreover, the pure oxygen is very reactive, and due to its specific physical properties (colorless, odorless, and tasteless), it cannot be detected by human senses. Therefore, many efforts have been made to produce low cost, faster, and linear oxygen gas sensors based on semiconductor nanostructures. These semiconductor gas sensors detect an oxidizing or reducing gas by observing change in electrical resistance. The surface area, size, and shape of nanostructures play an important role in the development of a gas sensor.[14] The nanofibers have a larger specific surface area than that of the micrometer-sized powders.[15] Further, the porous nature of nanofibers facilitates the gas diffusion, and chain like nanofibers provide a continuous path for charge transport.[16−18] This unique morphology increases the electrochemical reaction sites. As a result, the sensor based on nanofibers morphology exhibits improved sensitivity, lower detection limits, and a faster response to the change in the gas concentration.

Titanium based oxides have been used to fabricate gas sensors due to their wide band gap (3.3−4.0 eV).[19,20] Castaneda reported the effect of palladium coatings on oxygen sensors of TiO_2 thin films prepared by the ultrasonic spray pyrolysis method.[21] He also investigated the effect of colloidal silver nanoparticles on the performance of the flower-like titanium-dioxide-nanostructure-based oxygen sensor.[22] Moreover, it has been observed that the addition of rhodium to TiO_2 films increases their sensitivity.[23] Furthermore, gas sensors based on nanofibers of various titanates have been investigated in recent years as well. Hu et al. reported a low temperature $SrTiO_3$ oxygen sensor by recording DC currents.[11] Choi et al. studied sensing properties of electrospun $SrTi_{0.65}Fe_{0.35}O_{3-\delta}$

Received: January 17, 2014
Accepted: February 24, 2014
Published: February 24, 2014

   dx.doi.org/10.1021/am500354a | ACS Appl. Mater. Interfaces 2014, 6, 4542−4549

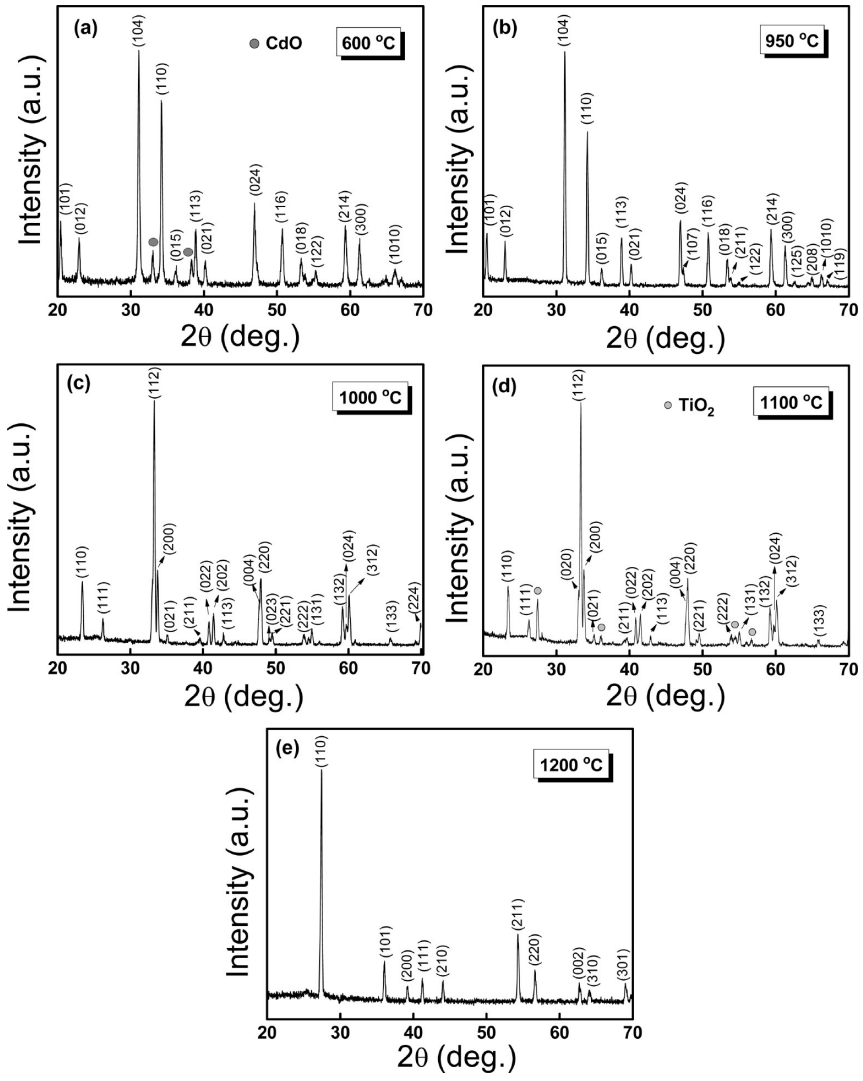

Figure 1. XRD patterns of the products obtained after heating at (a) 600 °C, (b) 950 °C, (c) 1000 °C, (d) 1100 °C, and (e) 1200 °C.

nanofibers using DC electrical measurements.[6] Ding et al. studied the gas sensors based on electrospun nanofibers and showed that nanofiber-based sensors have much higher sensitivity and quicker responses to target gases.[24]

However, there are no studies on gas sensing characteristics of $CdTiO_3$ nanofibers. Furthermore, the effect of annealing on change in surface area, grain size, and sensing properties of $CdTiO_3$ nanofibers has not been investigated as well. Therefore, we investigate the changes in surface area and grain size of $CdTiO_3$ nanofibers upon annealing and its effect on oxygen sensing. Annealing at 600 °C, 950 °C, 1000 °C, and >1100 °C resulted in ilmenite $CdTiO_3$ nanofibers with a very small amount of CdO, pure ilmenite $CdTiO_3$ nanofibers, pure perovskite $CdTiO_3$ nanofibers, and rutile TiO_2 nanofibers, respectively. BET analysis showed that with an increase in annealing temperature, the surface area of nanofibers decreases. The $CdTiO_3$ nanofibers annealed at 600 °C (ilmenite) and 1000 °C (perovskite) were then used to fabricate oxygen sensors. Better oxygen characteristics of ilmenite nanofibers were observed as compared to the perovskite nanofiber sensor and are attributed to their large surface area and porosity.

2. MATERIALS AND METHODS

2.1. Nanofiber Synthesis and Characterization. $CdTiO_3$ nanofibers were prepared via the electrospinning technique.[10] Cadmium acetate ($Cd(CH_3COO)_2{\cdot}2H_2O$ > 98%), titanium tetraisopropoxide ($Ti(CH_3)_2CHO)_4$ > 99%), acetic acid (CH_3COOH >98%), ethanol (C_2H_5OH >98%), and polyvinyl-pyrrolidone (PVP; M_W = 1 300 000) were purchased from Sigma-Aldrich. All chemicals were used without any further purification and were of analytical grade. Solution one was prepared by adding 2 g of cadmium acetate in 4 mL of acetic acid at room temperature. Titanium tetraisopropoxide was then mixed dropwise in solution 1. The second solution was prepared by adding 0.5 g of PVP in 4 mL of ethanol under stirring for 15 min. To get a homogeneous solution of optimum viscosity, these two solutions were mixed and vigorously stirred for 3 h in a glovebox.

The final solution was loaded in a syringe with a 24-gauge needle. The needle and collector plates were connected to the positive and negative terminals of a high voltage power supply of 10 kV, respectively. The nanofibers were collected on aluminum foil placed on the collector plate. The distance between the tip of the needle and collector plate was 7 cm, resulting in an electric field of 1.42 kV/cm. The whole process of electrospinning was carried out in an open environment. The as-spun nanofibers were dried in an oven at 80 °C for 3 h. Finally, PVP was burned to obtain pure $CdTiO_3$ nanofibers by annealing at different temperatures from 600 to 1200 °C for 3 h at a heating rate of 5 °C/min.

dx.doi.org/10.1021/am500354a | ACS Appl. Mater. Interfaces 2014, 6, 4542−4549

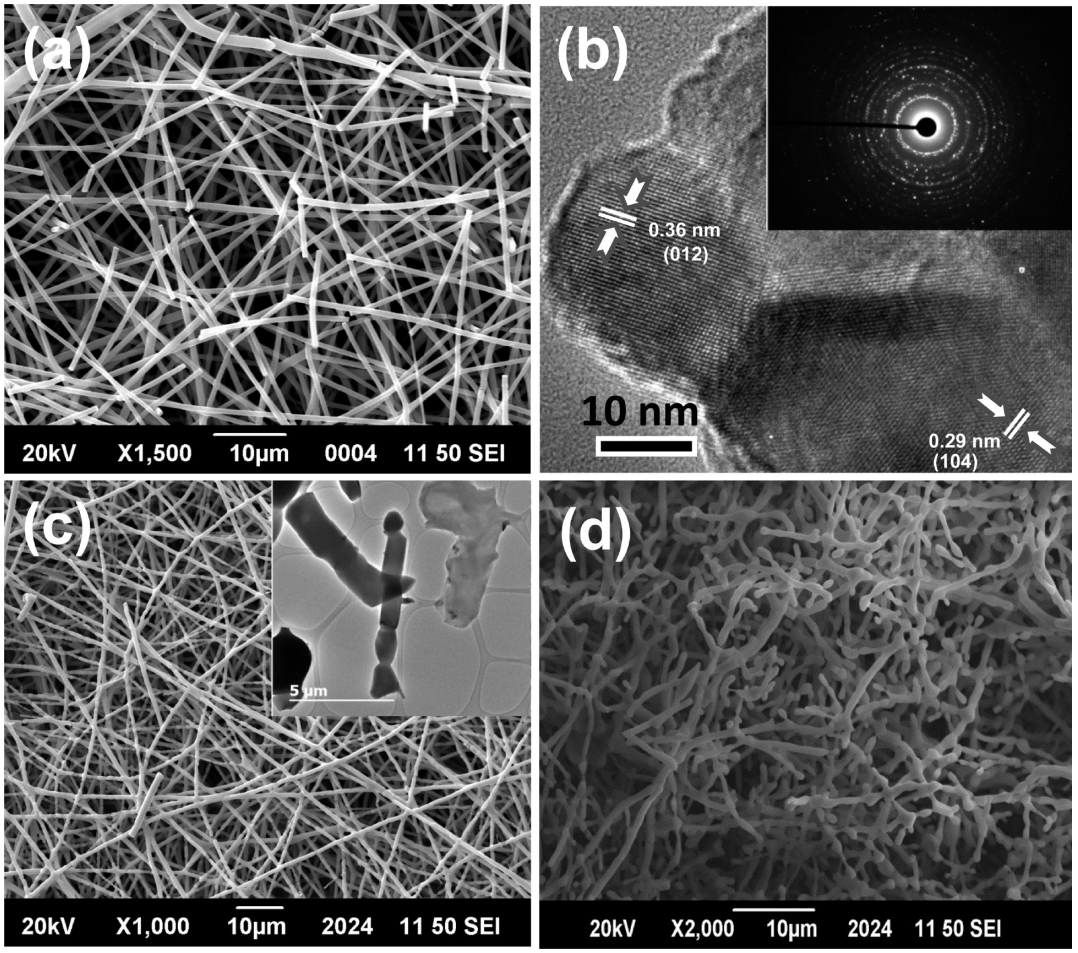

Figure 2. (a) SEM image of $CdTiO_3$ nanofibers annealed at 600 °C. (b) HRTEM image of $CTiO_3$ nanofibers annealed at 600 °C (inset shows the SAED image). (c) SEM image of $CdTiO_3$ nanofibers annealed at 1000 °C (inset shows the TEM image). (d) SEM image of $CdTiO_3$ nanofibers annealed at 1200 °C.

2.2. Device Fabrication. To study the oxygen sensing properties, suspension of the $CdTiO_3$ nanofibers with an ilmenite phase (annealed at 600 °C) and perovskite phase (annealed at 1000 °C) in isopropanol was prepared with a weight ratio of 1:100. The suspension was placed in an ultrasonic bath for 30 min to disperse nanofibers uniformly in isopropanol. Two different devices were then fabricated on a glass substrate using ilmenite and perovskite nanofibers. First of all, lithography and thermal evaporation were used to define electrical contacts with a separation of ~80 μm between them. Chromium (20 nm) followed by gold (80 nm) was evaporated for the contacts. Subsequently, nanofibers were deposited between the electrical contacts on a glass substrate by dropping a known volume of nanofiber suspension using a micropipet. As a result, multiple nanofibers were randomly deposited between the electrodes. Since the same volume of suspension was used, the number of nanofibers between electrical contacts was approximately the same in both devices.

2.3. Characterization. X-ray diffraction (XRD) analysis was performed using a D8 Discoverer HR-XRD BRUKER (Germany) with Cu Kα radiation (λ = 1.5418 Å). Field emission scanning electron microscope (SEM) and transmission electron microscope (TEM) images were obtained on a JSM-6490LA SEM and a Jeol 2010 (200 kV) TEM Japan, respectively. BET analysis was performed on a Micromeretics ASAP 2020 apparatus. The BET specific surface area, pore volume, and pore size distribution of the annealed samples at 600 and 1000 °C were determined by N_2 adsorption−desorption isotherms at 77 K shown in Figure 3a and b. Both the annealed samples were degassed at 393 K for 6 h under a vacuum (3×10^{-1} Torr) before recording their BET isotherms. The cumulative pore volume was calculated from the amount of nitrogen adsorbed up to a relative pressure, P/P_0, of 0.99, assuming all the pores are filled. The working principle of BET surface area analysis can be found elsewhere.[25]

Oxygen sensing (99.9% pure) was studied using both devices at different gas flow rates. Oxygen flow was regulated by a 65 mm EW-32044-00 Cole-Parmer flow meter. It can precisely control the oxygen gas flow in the range of 0.44 to 5.05 sccm (standard cubic centimeter per minute). The performance of the gas sensing device was evaluated by taking DC measurements. Current−voltage (I−V) measurements were performed using a Keithley 2400 source meter. The complete setup for the gas sensor was maintained at ~25 °C in a clean-room environment.

3. RESULTS AND DISCUSSION

3.1. X-Ray Diffraction Study. Figure 1 shows the XRD spectra of $CdTiO_3$/PVP nanofiber mats. The nanofiber mats were dried at 200 °C in an oven for 1 h to remove the moisture and for easy removal of mats from the aluminum foil. The mats were then annealed at different temperatures for 3 h to remove the PVP and other solvents. The polycrystalline structure achieved at 600 °C is of the ilmenite rhombohedral phase with some impurity peaks of CdO. The peaks of CdO are present at 2θ = 33.06 and 38.34 as indicated in Figure 1a. The XRD pattern agrees with JCPDS Card no. 29-0277. The reflections were indexed in the ilmenite rhombohedral symmetry with lattice constant parameters a = 5.29 Å and c = 14.87 Å. To get a

dx.doi.org/10.1021/am500354a | ACS Appl. Mater. Interfaces 2014, 6, 4542−4549

pure ilmenite phase, we annealed the sample at different temperatures. We observed that at 950 °C the material yields the pure ilmenite phase. At this temperature, all of the traces of CdO are removed. The peaks shown in Figure 1b are indexed to the pure ilmenite phase of $CdTiO_3$ in space group $R\bar{3}$ (JCPDs card no. 29-0277). The presence of a new phase, recognized as orthorhombic $CdTiO_3$, was achieved at 1000 °C as shown in Figure 1c. At this temperature, no peaks of possible impurity phases such as TiO_2 and CdO are visible. All the diffraction peaks are indexed successfully according to the pure orthorhombic phase of $CdTiO_3$ with JCPDs card no. 78-1015 in space group *Pbn*21. The lattice constant parameters are a = 5.30 Å, b = 5.32 Å, and c = 7.67 Å. Further annealing at 1100 °C, the traces of rutile TiO_2 were observed in the orthorhombic $CdTiO_3$ as shown in Figure 1d. This may be due to the volatilization of cadmium at a relatively high temperature.[26] The sample annealed at 1200 °C shows the cadmium free pure rutile TiO_2 phase as shown in Figure 1e. All the diffraction peaks were indexed to a rutile phase of TiO_2 (JCPDs 72-1148) in space group *P*42/*mnm*. The lattice constant parameters are a = 4.59 Å and c = 2.96 Å. This confirms the complete cadmium volatilization.

The diffraction peaks in the X-ray patterns indicate a random or preferential growth of polycrystalline samples. To describe the preferential orientation, the texture coefficient (TC_{hkl}) was calculated by using equation[27]

$$TC_{hkl} = \frac{I_{hkl}/I_{r(hkl)}}{1/n \sum_n (I_{hkl}/I_{r(hkl)})} \quad (1)$$

where I_{hkl} indicates the intensities obtained from the X-ray diffraction pattern of nanofiber mats and n is the number of diffraction peaks taken into account. $I_{r(hkl)}$ is the intensity of the reference pattern (JCPDs card). The deviation of TC_{hkl} from unity or higher value implies the growth in the preferred orientation. This means that the growth in the preferred orientation is associated with the increased number of grains along that plane.[28] TC_{hkl}'s calculated for the nanofiber mats of different phases are shown in Table S (Supporting Information). It can be seen from Table S that the highest value of TC_{hkl} obtained from the ilmenite phase (950 °C) is 1.49 associated with the (012) plane, the orthorhombic phase (1000 °C) is 1.26 associated with the (113) plane, and rutile TiO_2 (1200 °C) is 1.60 associated with the (002) plane.

3.2. SEM and TEM Study. Figure 2 shows the morphologies of the $CdTiO_3$ nanofibers as a function of annealing temperature. After annealing at 600 °C, the average diameter of the nanofibers is ∼200 nm as shown in Figure 2a. The surface of the nanofibers annealed at this temperature is seen to be porous in nature. The HRTEM image of nanofibers annealed at 600 °C is shown in Figure 2b. From Figure 2b, it is observed that the nanofibers are composed of fine and closely linked grains ∼25 nm in size. The HRTEM image (Figure 2b) shows well-resolved lattice fringes. The distance between the adjacent lattice fringes is 0.36 and 0.29 nm, which corresponds to the interplanar spacing of $CdTiO_3$ (012) and (104) planes, respectively. Which agrees well with the d (012) and (104) spacing of the literature value (0.38 and 0.28 nm; JCPDS no. 29-0277). The corresponding selected area electron diffraction (SAED) pattern (inset of Figure 2b) of the nanofibers indicates clearly that nanofibers are polycrystalline. All of the diffraction rings can be indexed to the ilmenite phase of $CdTiO_3$ with rhombohedral structure. Figure 2c and d shows the SEM image of the sample annealed at 1000 and 1200 °C. The average diameter of nanofibers annealed at 1000 and 1200 °C is ∼600 nm and ∼800 nm, respectively. The inset of Figure 2c shows the TEM image of the sample annealed at 1000 °C. At an annealing temperature of 1000 and 1200 °C, the grain growth took place. The grain growth is pinned by thermal grooving in fibers. The grain size is about the same as the fiber diameter and leaves less pores as compared to 600 °C. The two mechanisms for thermal grooving were explained by Mullins.[29] One is the evaporation−condensation and the other is the surface diffusion. In our case, the nanofibers have a large pore size (∼19 nm). It is reported that the diffusion rate is high on the surface with large pore size.[30] This can explain that the inner surfaces of the nanofibers are utilized for gas detection. Therefore, we believe that surface diffusion is dominant in our case. The same mechanism was also suggested for zirconia nanofibers.[31]

3.3. BET Characterization. The BET surface area values calculated are 9.41 and 0.4 m^2/g for ilmenite and perovskite phases, respectively. As expected, the high temperature calcination step has reduced the surface area and porosity of the material. Surface area determined using BET is closely related to the average diameter of the nanofibers. As the diameter increases, the specific surface area also decreases. The extracted parameters from BET data are shown in Table 1.

Table 1. Surface Area, Pore Volume, Response Time, and Recovery Time for Both the Phases

sample	surface area (m^2/g)	pore volume (cm^3/g)	response time	recovery time
Ilmenite phase	9.41	0.04	∼120 s	∼23 s
Perovskite phase	0.40	0.02	∼156 s	∼50 s

3.4. Oxygen Sensing. Figure 4a and b shows room temperature $I-V$ characteristics of $CdTiO_3$ nanofiber sensors at different oxygen flow rates. Greater flow rate means greater oxygen concentration in the measurement chamber. As oxygen flow rate increases, current decreases in both ilmenite and perovskite nanofiber sensors. However, at 2.5 V, the change in current is greater for the ilmenite nanofibers sensor as compared to that in the perovskite nanofibers sensor. Figure 4c shows the relationship between oxygen flow rate and current at 2 V.

The DC electrical measurements have been employed widely to investigate the electronic and sensing properties in different oxide nanostructures at room temperature.[32−34] The hydrophilic surface of oxide nanofibers attracts hydrophilic contents (OH^-, H_2O, O^-, O_2^-, and O_2) from the surrounding environment.[35] Increase in hydrophilic contents or adsorption of hydrophilic contents on the surface of nanofibers result in increased sensing properties.

Oxygen sensing is mainly due to the surface oxygen chemisorption, which causes the formation of oxygen adsorbate (acceptor like states) on the surface. The $CdTiO_3$ surface contains the number of oxygen related physisorption and chemisorption species (hydrophilic contents).[21] The dominant species are atomic O^- and molecular O_2^- ions. Generally, below 150 °C, the molecular ions are dominant, whereas above this temperature the atomic ions take part[36,37] in sensing. These dominant species are negatively ionized. In the case of n-type semiconductor metal oxide, oxygen chemisorption extracts

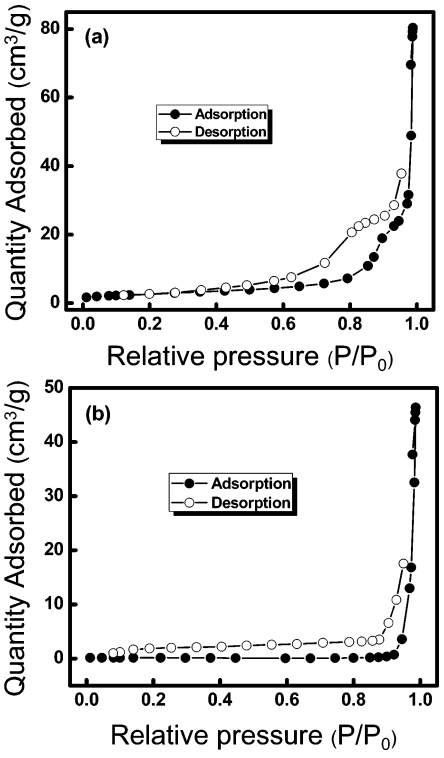

Figure 3. Nitrogen adsorption−desorption analysis of $CdTiO_3$ nanofibers annealed at (a) 600 °C and (b) 1000 °C.

electrons from the bulk and builds a space-charge layer (L) on the nanofibers surface. This creation of acceptor like states on the surface of $CdTiO_3$ can help in trapping of electrons. This causes a decrease in the majority carriers (electrons) that lead to an increase in electrical resistance.[12] The chemical reactions are described by the following equations:

$$O_2\ (\text{gas}) \rightarrow O_2\ (\text{adsorbed}) \tag{2}$$

$$O_2\ (\text{adsorbed}) + e^- \rightarrow O_2^-\ (\text{adsorbed}) \tag{3}$$

$$O_2^-\ (\text{adsorbed}) + e^- \rightarrow 2O^- \tag{4}$$

$$O^- + e^- \rightarrow O^{2-} \tag{5}$$

The working and response of the sensor usually depend on the thickness of the space-charge layer (L) formed from the O^- and O_2^- ions and on the grain size or the crystallite size (D) of the sensing material. The relationship of crystallite size and space charge layer can be defined in three different following ways. (*i*) When the grain size of the material is small enough ($D < 2L$), conductivity will be controlled by the grain itself, and the surface conduction mechanism is dominant in this case. This condition is suitable in nanocrystalline materials for gas sensor applications.[19] (*ii*) When crystalline size and space charge depth is comparable ($D \geq 2L$), the space-charge depth around grains forms a restricted neck, and this neck acts as a potential barrier, and this makes conduction difficult. In this case, the conduction mechanism usually is controlled by the grain boundaries. (*iii*) When the grain size is large enough ($D \gg 2L$), the conductivity will depend on the inner mobile charge carriers, and the conductivity depends on the barrier height.

The average grain size of the $CdTiO_3$ nanofibers with the ilmenite phase annealed at 600 °C is ∼25 nm. The L of the chemisorbed oxygen range is normally ∼10^2 to 10^3 nm for the

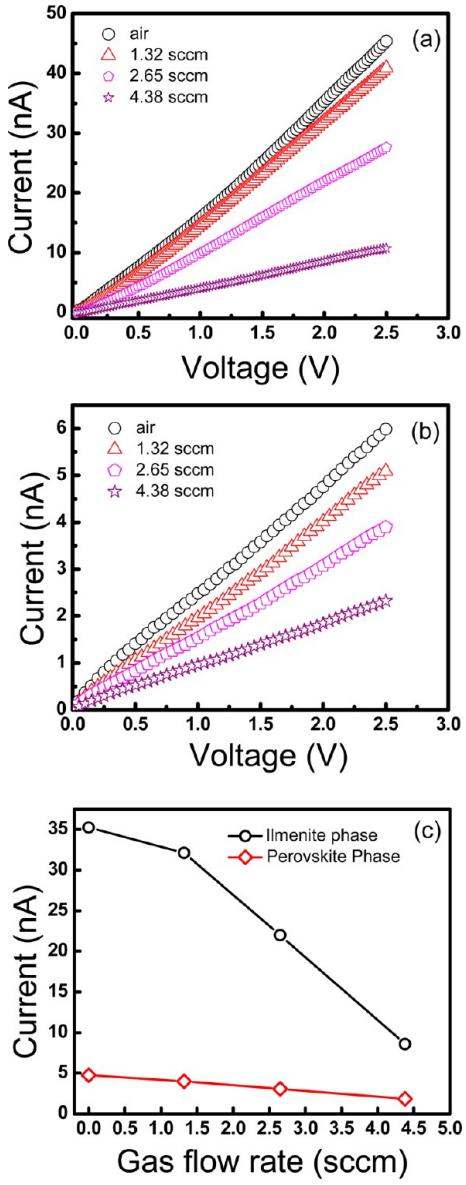

Figure 4. *I*−*V* characteristics of $CdTiO_3$ nanofibers gas sensing device at different oxygen flow rates. (a) Ilmenite phase, (b) perovskite phase, and (c) relationship between oxygen flow rate and current calculated at 2 V.

semiconducting oxide materials.[38] Hence, as discussed earlier, surface conduction is dominant in this case ($D < 2L$), and therefore the surface-to-bulk ratio of the material is much greater than that of coarse material.[39] Therefore, the grain size of the material is very important to controlling the gas sensing properties of the material. Upon annealing at 1000 °C, the material changes to neck control type ($D \geq 2L$).[40,41] So conduction is controlled by grain boundaries. Figure 5 shows the schematic representation of $CdTiO_3$ nanofibers showing the effect of the crystallite size on the sensitivity of a gas sensing device.

Gas response is defined as the ratio of the resistance change of a sensor upon exposure to a sample gas to its original resistance:

$$\text{gas response} = \frac{R_g}{R_o} - 1\ R_g > R_o \tag{6}$$

dx.doi.org/10.1021/am500354a | ACS Appl. Mater. Interfaces 2014, 6, 4542−4549

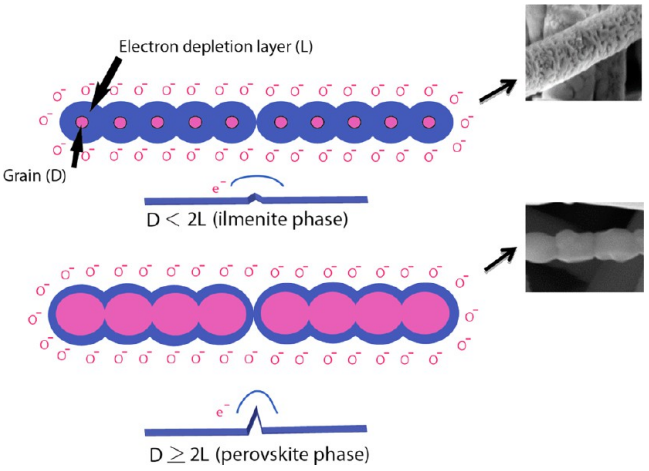

Figure 5. Schematic representation of $CdTiO_3$ nanofibers showing the effect of the crystallite size on the sensitivity of oxygen sensor sensing devices.

$$\text{gas response} = 1 - \frac{R_g}{R_o} \quad R_o > R_g \tag{7}$$

where R_o is the resistance in air and R_g is the resistance in a sample gas.[41] Figure 6a compares the gas response of ilmenite

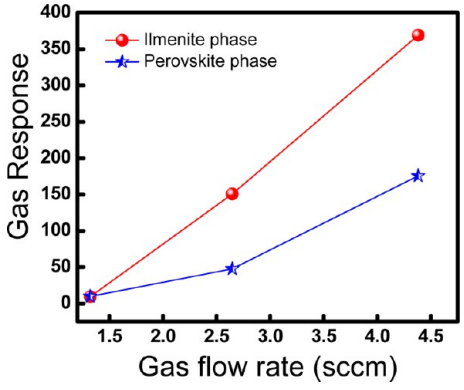

Figure 6. Gas response variation of $CdTiO_3$ nanofibers as a function of oxygen flow rates.

and perovskite $CdTiO_3$ nanofiber sensors at different oxygen flow rates. The gas response increased as the oxygen flow rate was increased for both the sensors. The perovskite nanofibers sensor showed a nonlinear response, whereas the ilmenite nanofibers sensor exhibited a linear response. At 4.38 sccm, the ilmenite nanofibers sensor exhibited a higher response as compared to the perovskite nanofibers sensor. This may be due to an increase in grain size and reduced pore size upon annealing at a temperature of 1000 °C. This also affects charge carrier concentration on the nanofiber surface.[12] The linear relationship between gas response and oxygen flow rate provides strong evidence for the availability of a sufficient number of sensing sites on the surface of nanofibers to interact with the oxygen.[42] In addition, the surface reaction increases with an increase in oxygen flow rate due to a large surface coverage. It can also be concluded from the linearity of the response curve with the oxygen flow rate that the sensor can be reliably used to monitor oxygen over this range.[43]

For practical applications, the response and recovery times of the gas sensors are very important. The response and recovery times of nanofiber sensors were recorded at 25 °C and 2 V and at an oxygen flow rate of 2.65 sccm. A complete recovery was observed after the removal of oxygen from the chamber. Figure 7a and b shows response time ($t_{(\text{air-to-oxygen})}$) and recovery time

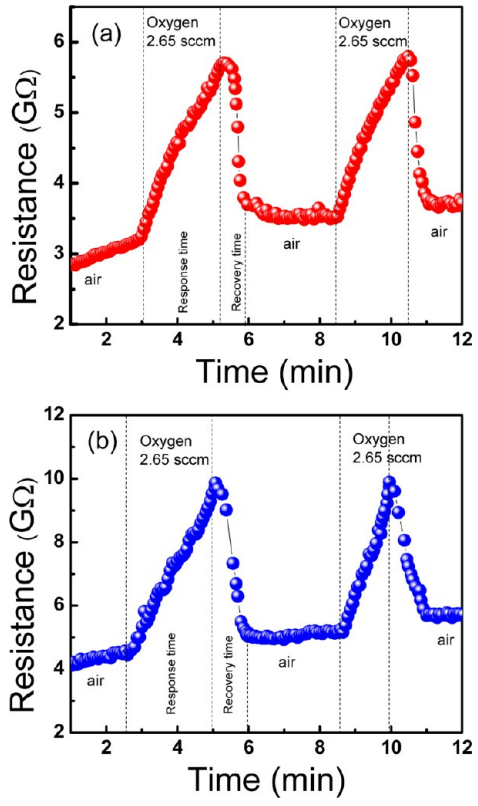

Figure 7. Response curves of $CdTiO_3$ nanofibers. (a) Ilmenite phase. (b) Perovskite phase.

($t_{(\text{oxygen-to-air})}$) for both the ilmenite and perovskite phases. It can be seen that results are reproducible for two complete response/recovery cycles. The response time and recovery time for both phases of nanofibers are listed in Table 1.

4. CONCLUSIONS

The phase transformations in $CdTiO_3$ nanofibers upon thermal annealing at different temperatures were studied. The pure ilmenite phase was achieved at 950 °C, whereas annealing at 1000 °C resulted in the pure perovskite phase. $CdTiO_3$ nanofibers were converted to the TiO_2 rutile phase at temperatures above 1100 °C. BET analysis indicated that the surface area of nanofibers decreases with an increase in annealing temperature. Oxygen sensors of $CdTiO_3$ nanofibers annealed at 600 °C (ilmenite) and 1000 °C (perovskite) were fabricated. Annealing caused changes in grain size, surface area, and porosity of nanofibers and therefore influenced the sensing properties of these nanofibers. The sensor based on ilmenite nanofibers (annealed at 600 °C) having a smaller grain size and higher surface area (9.41 m^2/g) was more sensitive and had a fast response as compared to the sensor based on perovskite nanofibers (annealed at 1000 °C). On exposure to gas, the adsorption of oxygen ions on the nanofiber surface reduces the electrons for conduction, causing an increase in resistance of the nanofibers. These results demonstrate that $CdTiO_3$ nanofibers with the ilmenite phase could be promising candidates for the fabrication of oxygen sensors.

■ ASSOCIATED CONTENT

Supporting Information

X-ray diffraction intensities and preferred orientation factor for ilmenite phase $CdTiO_3$, perovskite phase $CdTiO_3$, and TiO_2. This material is available free of charge via the Internet at http://pubs.acs.org.

■ AUTHOR INFORMATION

Corresponding Author

*Phone:+92-51-2207381. Fax: +92-51-2208070. E-mail: aftab@cantab.net.

Notes

The authors declare no competing financial interest.

■ ACKNOWLEDGMENTS

We acknowledge the financial support of the Higher Education Commission (HEC), Pakistan.

■ REFERENCES

(1) Pavasupree, S.; Laosiripojana, N.; Chuangchote, S.; Sagawa, T. Fabrication and Utilization of Titania Nanofibers from Natural Leucoxene Mineral in Photovoltaic Applications. *Jpn. J. Appl. Phys.* **2011**, *50* (1), 1−4.

(2) Watthanaarun, J.; Pavarajarn, V.; Supaphol, P. Titanium (IV) oxide nanofibers by combined sol-gel and electrospinning techniques: preliminary report on effects of preparation conditions and secondary metal dopant. *Sci. Technol. Adv. Mater.* **2005**, *6* (3−4), 240−245.

(3) Zhang, D.; Yoshida, T.; Minoura, H. Low Temperature Fabrication of Efficient Porous Titania Photoelectrodes by Hydrothermal Crystallization at the Solid/Gas Interface. *Adv. Mater.* **2003**, *15* (10), 814−817.

(4) Yun, H. S.; Miyazawa, K. C.; Honma, I.; Zhou, H.; Kuwabara, M. Synthesis of semicrystallized mesoporous TiO_2 thin films using triblock copolymer templates. *Mater. Sci. Eng., C* **2003**, *23* (4), 487−494.

(5) Viseu, T. M. R.; Ferreira, M. I. C. Morphological characterization of TiO_2 thin films. *Vacuum* **1999**, *52* (1−2), 115−120.

(6) Choi, S. H.; Choi, S. J.; Min, B. K.; Lee, W. Y.; Park, J. S.; Kim, I. D. Facile Synthesis of p-type Perovskite $SrTi_{0.65}Fe_{0.35}O_{3-delta}$ Nanofibers Prepared by Electrospinning and Their Oxygen-Snsing Properties. *Macromol. Mater. Eng.* **2012**, *298*, 521−527.

(7) Castañeda, L.; Alonso, J. C.; Ortiz, A.; Andrade, E.; Saniger, J. M.; Bañuelos, J. G. Spray pyrolysis deposition and characterization of titanium oxide thin films. *Mater. Chem. Phys.* **2002**, *77* (3), 938−944.

(8) Castañeda, L.; Terrones, M. Synthesis and structural characterization of novel flower-like titanium dioxide nanostructures. *Phys. B (Amsterdam, Neth.)* **2007**, *390* (1−2), 143−146.

(9) Tai, W. P.; Oh, J. H. Fabrication and humidity sensing properties of nanostructured TiO_2-SnO_2 thin films. *Sens. Actuators, B* **2002**, *85* (1−2), 154−157.

(10) Imran, Z.; Batool, S. S.; Israr, M. Q.; Sadaf, J. R.; Usman, M.; Jamil, H.; Javed, M. Y.; Rafiq, M. A.; Hasan, M. M.; Nur, O.; Willander, M. Fabrication of cadmium titanate nanofibers via electrospinning technique. *Ceram. International* **2012**, *38* (4), 3361−3365.

(11) Hu, Y.; Tan, O. K.; Pan, J. S.; Huang, H.; Cao, W. The effects of annealing temperature on the sensing properties of low temperature nano-sized $SrTiO_3$ oxygen gas sensor. *Sens. Actuators, B* **2005**, *108* (1), 244−249.

(12) Lu, H. F.; Li, F.; Liu, G.; Chen, Z.-G.; Wang, D.-W.; Fang, H.-T.; Lu, G. Q.; Jiang, Z. H.; Cheng, H.-M. Amorphous TiO_2 nanotube arrays for low-temperature oxygen sensors. *Nanotechnology* **2008**, *19* (40), 405504.

(13) Neri, G.; Bonavita, A.; Micali, G.; Rizzo, G.; Pinna, N.; Niederberger, M. In_2O_3 and Pt-In_2O_3 nanopowders for low temperature oxygen sensors. *Sens. Actuators, B* **2007**, *127* (2), 455−462.

(14) Pawar, R. C.; Lee, J.-W.; Patil, V. B.; Lee, C. S. Synthesis of Multi-dimensional ZnO nanostructures in aqueous medium for the application of gas sensor. *Sens. Actuators, B* **2012**, *187*, 323−330.

(15) Yang, M.; Wang, J.; Li, H.; Zheng, J.-G.; Wu, N. N. A lactate electrochemical biosensor with a titanate nanotube as direct electron transfer promoter. *Nanotechnology* **2008**, *19* (7), 075502.

(16) Zhi, M.; Koneru, A.; Yang, F.; Manivannan, A.; Li, J.; Wu, N. Electrospun $La_{0.8}Sr_{0.2}MnO_3$ nanofibers for a high-temperature electrochemical carbon monoxide sensor. *Nanotechnology* **2012**, *23* (30), 305501.

(17) Zhi, M.; Mariani, N.; Gemmen, R.; Gerdes, K.; Wu, N. Nanofiber scaffold for cathode of solid oxide fuel cell. *Energy Environ. Sci.* **2011**, *4* (2), 417−420.

(18) Wang, D.; Zhao, H.; Wu, N.; El Khakani, M. A.; Ma, D. Tuning the charge-transfer property of PbS-quantum dot/TiO_2-nanobelt nanohybrids via quantum confinement. *J. Phys. Chem. Lett.* **2010**, *1* (7), 1030−1035.

(19) Sun, Y. F.; Liu, S. B.; Meng, F. L.; Liu, J. Y.; Jin, Z.; Kong, L. T.; Liu, J. H. Metal oxide nanostructures and their gas sensing properties: a review. *Sensors* **2012**, *12* (3), 2610−2631.

(20) Murugadoss, G. Synthesis and Characterization of Transition Metals Doped ZnO Nanorods. *J. Mater. Sci. Technol.* **2012**, *28* (7), 587−593.

(21) Castaneda, L. Effects of palladium coatings on oxygen sensors of titanium dioxide thin films. *Mater. Sci. Eng., B* **2007**, *139* (2), 149−154.

(22) Castañeda, L. Influence of colloidal silver nanoparticles on the performance of novel flower-like titanium dioxide oxygen sensor. *Sens. Mater.* **2009**, *21* (1), 25−36.

(23) Castañeda, L.; Maldonado, A.; de la L. Olvera, M. Sensing properties of chemically sprayed TiO_2 thin films using Ni, Ir, and Rh as catalysts. *Sens. Actuators, B* **2008**, *133* (2), 687−693.

(24) Ding, B.; Wang, M.; Yu, J.; Sun, G. Gas sensors based on electrospun nanofibers. *Sensors* **2009**, *9* (3), 1609−1624.

(25) Timmermann, E. O. Multilayer sorption parameters: BET or GAB values? *Colloids Surf., A* **2003**, *220* (1), 235−260.

(26) Gupta, V.; Bamzai, K. K.; Kotru, P. N.; Wanklyn, B. M. Dielectric properties, ac conductivity and thermal behaviour of flux grown cadmium titanate crystals. *Mater. Sci. Eng., B* **2006**, *130* (1), 163−172.

(27) Mohamed, S. H. SnO_2 dendrites-nanowires for optoelectronic and gas sensing applications. *J. Alloys Compd.* **2012**, *510* (1), 119−124.

(28) Lv, J.; Liu, C.; Gong, W.; Zi, Z.; Chen, X.; Chen, X.; Huang, K.; He, G.; Shi, S.; Song, X. Study of near white light emission for ZnO thin films grown on silicon substrates. *Semicond. Sci. Technol.* **2012**, *27* (11), 115021.

(29) Mullins, W. W. Theory of thermal grooving. *J. Appl. Phys.* **1957**, *28* (3), 333−339.

(30) Yeow, S. C.; Ong, W. L.; Wong, A. S. W.; Ho, G. W. Template-free synthesis and gas sensing properties of well-controlled porous tin oxide nanospheres. *Sens. Actuators, B* **2009**, *143* (1), 295−301.

(31) Li, L.; Zhang, P.; Liang, J.; Guo, S. M. Phase transformation and morphological evolution of electrospun zirconia nanofibers during thermal annealing. *Ceram. International* **2010**, *36* (2), 589−594.

(32) Baratto, C.; Sberveglieri, G.; Onischuk, A.; Caruso, B.; Di Stasio, S. Low temperature selective NO_2 sensors by nanostructured fibres of ZnO. *Sens. Actuators, B* **2004**, *100* (1), 261−265.

(33) Hu, Y.; Tan, O. K.; Cao, W.; Zhu, W. Fabrication and characterization of nano-sized $SrTiO_3$-based oxygen sensor for near room-temperature operation. *IEEE Sensors J.* **2005**, *5* (5), 825−832.

(34) Fan, Z.; Wang, D.; Chang, P.-C.; Tseng, W.-Y.; Lu, J. G. ZnO nanowire field-effect transistor and oxygen sensing property. *Appl. Phys. Lett.* **2004**, *85*, 5923.

(35) Rasool, K.; Rafiq, M. A.; Li, C. B.; Krali, E.; Durrani, Z. A. K.; Hasan, M. M. Enhanced electrical and dielectric properties of polymer covered silicon nanowire arrays. *Appl. Phys. Lett.* **2012**, *101* (2), 023114−023114−4.

(36) Tricoli, A.; Righettoni, M.; Teleki, A. Semiconductor gas sensors: Dry synthesis and application. *Angew. Chem., Int. Ed. Engl.* **2010**, *49* (42), 7632−7659.

(37) Barsan, N.; Weimar, U. Conduction model of metal oxide gas sensors. *J. Electroceram.* **2001**, *7* (3), 143−167.
(38) Kohl, D. Surface processes in the detection of reducing gases with SnO_2-based devices. *Sens. Actuators* **1989**, *18* (1), 71−113.
(39) Martinelli, G.; Carotta, M. C.; Traversa, E.; Ghiotti, G. Thick-film gas sensors based on nano-sized semiconducting oxide powders. *MRS Bull.* **1999**, *24* (6), 30−35.
(40) Shimizu, Y.; Egashira, M. Basic aspects and challenges of semiconductor gas sensors. *MRS Bull.* **1999**, *24* (6), 18−24.
(41) Wagh, M. S.; Jain, G. H.; Patil, D. R.; Patil, S. A.; Patil, L. A. Modified zinc oxide thick film resistors as NH_3 gas sensor. *Sens. Actuators, B* **2006**, *115* (1), 128−133.
(42) Moos, R.; Izu, N.; Rettig, F.; Sebastian, R.; Shin, W.; Matsubara, I. Resistive oxygen gas sensors for harsh environments. *Sensors* **2011**, *11* (4), 3439−3465.
(43) Souri, M.; Azarmanesh, M.; Sani, E. A.; Nasseri, M.; Farhadi, K. An analytical study of resistive oxygen gas sensors. *J. Phys.: Condens. Matter* **2008**, *20* (14), 145204.